Cranfield
COA REPORT No. 9308
June, 1993

FULLY DISCRETE HIGH-ORDER TVD SCHEMES FOR A SCALAR HYPERBOLIC CONSERVATION LAW

J.Shi and E.F.Toro

DEPARTMENT OF AEROSPACE SCIENCE
COLLEGE OF AERONAUTICS
CRANFIELD INSTITUTE OF TECHNOLOGY
CRANFIELD, MK43 OAL, U.K.

Cranfield

College of Aeronautics Report No 9308
June 1993

FULLY DISCRETE HIGH-ORDER TVD SCHEMES FOR A SCALAR HYPERBOLIC CONSERVATION LAW

J. Shi and E. F. Toro

College of Aeronautics
Cranfield Institute of technology
Cranfield, Bedford MK43 0AL. England

ISBN 1 871564 64 6

£10.00

Abstract

In this paper we investigate fully discrete high-order TVD schemes for a scalar hyperbolic conservation law using flux limiters . Formulae which define Courant number dependent TVD regions for second and third-order TVD schemes are established. A semi-empirical TVD procedure for an m-th order scheme ($m \geq 4$) are proposed and tested.

1 Introduction

An important research subject in Computational Fluid Dynamics (CFD) concerns the development of high-order numerical schemes. There are many application areas for which such research is of vital importance. One example of considerable interest is Acoustics, which needs long time evolution of weak flow features. For this kind of problems low-order methods will produce unacceptable dispersive and diffusive errors in a very short time. Another example concerns problems containing weak shocks in which the physical effects of diffusion and dispersion are important mechanisms. Low-order methods contain large amounts of numerical diffusion and dispersion and are thus totally inaccurate for simulating the propagation of weak shocks. In large computational problems low-order methods would require vast amounts of computer memory (possibly not available in current computers) in order to attain a satisfactory degree of accuracy. A high-order method would attain the same accuracy with coarser meshes requiring less sophisticated hardware and making it possible to actually run the problems.

Essentially, there are two different techniques to construct high-order numerical schemes: semi-discrete and fully discrete methods. In the semi-discrete method [1] one divides the discretization process into two separate stages. In the first stage one discretizes in space only leaving the problem continuous in time; in the second stage one has sets of Ordinary Differential Equations (ODE) in time, which can be discretized appropriately. Often this technique is called **the method of lines.** The MUSCL approach introduced by van Leer [2] can be utilised in conjunction with the method of lines. The recently developed ENO schemes [3]-[5] belong to this category. The main idea of the ENO scheme is that the spacial high-order approximations to the flux at a cell interface can be defined using high-order interpolation in space, and then the high-order temporal accuracy can be achieved by another discretization applying a high-order ODE solver.

In [6] Shi and Toro proposed a fully discrete technique to construct schemes of arbitrary accuracy and as examples presented fully discrete second, third, and fourth-order schemes for linear model hyperbolic conservation law. The approach is based

on Taylor expansion in both space and time in a single stage. The stability analyses of the high-order schemes were conducted by using a simplified Von Neumann method [7].

We are interested in methods for computing discontinuous solution, for which all high-order methods are inadequate, i.e. they produce spurious oscillations near discontinuities. In this paper we modify the high-order schemes presented in [6] so as to avoid the spurious oscillations and preserve high-order accuracy in smooth parts of the flow. We achieve this by imposing a Total Variation Diminishing (TVD) constraint [8] via the introduction of flux limiter function [9]. For second and third-order accurate schemes we carry out a rigorous TVD analysis that results in Courant-number dependent TVD regions. Flux limiters are constructed and tested. For methods of fourth or higher order of accuracy we propose a semi-empirical TVD approach that works well; it is based on the theory for third-order schemes. Collective experience with second-order methods suggest that this analysis might provide a useful guide for constructing schemes to solve non-linear systems.

The rest of this paper is as follows: in section 2 we investigate the TVD theory for fully discrete schemes; in section 3 we apply this theory to derive Courant-number dependent TVD regions and to construct and test limiter function for second-order methods; in section 4 we apply the theory to third-order fully discrete schemes. In section 5 we investigate a procedure to develop TVD versions of schemes of arbitrary-order accuracy; as an example we construct fourth-order TVD schemes. Conclusions are dramn in section 6.

2 High-order TVD Formula

We consider the initial value problem (IVP) for one dimensional scalar hyperbolic conservation laws, namely

$$\begin{aligned} u_t + f(u)_x &= 0 \qquad -\infty < x < \infty, t \geq 0 \\ u(x,0) &= u_0(x) \end{aligned} \tag{1}$$

Here, u is the unknown function and $f(u)$ is the physical flux.

In this paper we take the linear case $f(u) = au$ so that $f'(u) = a$ is a constant wave propagation speed.

We discretise the computational half plane by choosing a uniform mesh with a mesh width $h = \triangle x$, a time step $k = \triangle t$ and define the computational grid $x_j = jh$, $t_n = nk$. We use U_j^n to denote the computed approximation to the exact solution $u(x_j, t_n)$ of equation (1).

We consider the conservative numerical schemes introduced in [6]

$$U_j^{n+1} = U_j^n - \frac{k}{h}[F(U^n; j) - F(U^n; j-1)] \tag{2}$$

with numerical flux

$$F(U^n; j) = \frac{1}{2}(F_j^n + F_{j+1}^n) - \frac{1}{2}|a|(U_{j+1}^n - U_j^n) + |a|\left(D_0 \Delta U_{j+\frac{1}{2}} + D_1 \Delta U_{j+L+\frac{1}{2}}\right) \tag{3}$$

where D_0 and D_1 are coefficients, and

$$\Delta U_{j+L+\frac{1}{2}} = U_{j+L+1}^n - U_{j+L}^n \tag{4}$$

$$\begin{cases} L = -1 & for \quad c > 0 \\ L = 1 & for \quad c < 0 \end{cases} \tag{5}$$

Here c is the Courant number defined as $c = \frac{ak}{h}$.

The above scheme includes three-point, second-order centered scheme, five-point, second-order upwind scheme and five-point, third-order scheme. For example, when D_1 is zero it reduces to the second-order Lax-Wendroff scheme; when D_0 is zero it gives the second-order Beam-warming scheme; for D_0 and D_1 distincting from zero it gives the five-point third-order scheme (see [6] for detail).

Imposing a TVD constraint on (3) via a flux limiter gives

$$F(U^n; j) = \frac{1}{2}(F_j^n + F_{j+1}^n) - \frac{1}{2}|a|(U_{j+1}^n - U_j^n) + |a|\left(D_0 \Delta U_{j+\frac{1}{2}} + D_1 \Delta U_{j+L+\frac{1}{2}}\right)\phi_j \tag{6}$$

where ϕ_j is a flux limiter.

Theorem 2.1 *Scheme (2) (6) is TVD for* $|c| \leq 1$ *if the flux limiter is determined by*

$$\phi_j \leq \frac{(1-|c|)\theta_j}{|c|(D_1\theta_j + D_0)} \tag{7}$$

$$\phi_j \leq \frac{\theta_j}{\theta_j D_1 + D_0} \tag{8}$$

$$\phi_j \leq \frac{1-|c|}{|c|(D_0 + D_1\theta_j)} \tag{9}$$

$$\phi_j \leq \frac{1}{D_0 + D_1\theta_j} \tag{10}$$

where

$$\phi_j = 0 \quad for \quad \theta_j \leq 0 \tag{11}$$

$$\theta_j = \frac{\Delta U_{j-\frac{1}{2}}}{\Delta U_{j+\frac{1}{2}}} \quad for \quad c > 0 \tag{12}$$

$$\theta_j = \frac{\Delta U_{j+\frac{3}{2}}}{\Delta U_{j+\frac{1}{2}}} \quad for \quad c < 0 \tag{13}$$

Proof

First consider a method with Courant number of $0 \leq c \leq 1$. From (2) and (6), the numerical method is

$$\begin{aligned} U_j^{n+1} = U_j^n - c\Big[&\Delta U_{j-\frac{1}{2}} + D_0 \Delta U_{j+\frac{1}{2}}\ \phi_j + D_1 \Delta U_{j-\frac{1}{2}}\ \phi_j - D_0 \Delta U_{j-\frac{1}{2}}\ \phi_{j-1} \\ &- D_1 \Delta U_{j-\frac{3}{2}}\ \phi_{j-1}\Big] \end{aligned} \tag{14}$$

Modifying equation (14), we get

$$\frac{U_j^{n+1} - U_j^n}{-\Delta U_{j-\frac{1}{2}}} = c\left[1 + \left(D_1 + D_0\frac{1}{\theta_j}\right)\phi_j - (D_0 + D_1\theta_{j-1})\phi_{j-1}\right] \tag{15}$$

We now apply the data compatibility condition of Roe [10] whereby the sufficient condition

$$0 \leq \frac{U_j^{n+1} - U_j^n}{-\Delta U_{j-\frac{1}{2}}} \leq 1 \tag{16}$$

offers the TVD requirement.

This is equivalent to the Harten's creterion [8] for a scheme written as

$$U_j^{n+1} = U_j^n - B_{j-1}\Delta U_{j-\frac{1}{2}} + D_j \Delta U_{j+\frac{1}{2}} \tag{17}$$

with the choice

$$B_{j-1} = c\left[1 + \left(D_1 + D_0\frac{1}{\theta_j}\right)\phi_j - (D_0 + D_1\theta_{j-1})\phi_{j-1}\right] \tag{18}$$

$$D_j = 0 \tag{19}$$

Harten's theorem requires

$$B_{j-1} \geq 0 \qquad \forall\, j \tag{20}$$

$$D_j \geq 0 \qquad \forall\, j \tag{21}$$

$$B_{j-1} + D_j \leq 1 \qquad \forall\, j \tag{22}$$

We apply condition (16) to (15), that is

$$0 \leq c\left[1 + \left(D_1 + D_0\frac{1}{\theta_j}\right)\phi_j - (D_0 + D_1\theta_{j-1})\phi_{j-1}\right] \leq 1 \tag{23}$$

To satisfy the inequality the following conditions have to hold

$$\left|\left(D_1 + D_0\frac{1}{\theta_j}\right)\phi_j - (D_0 + D_1\theta_{j-1})\phi_{j-1}\right| \leq \frac{1-c}{c} \tag{24}$$

$$\left|(D_0 + D_1\theta_{j-1})\phi_{j-1} - \left(D_1 + D_0\frac{1}{\theta_j}\right)\phi_j\right| \leq 1 \tag{25}$$

i.e.

$$0 \leq \left(D_1 + D_0\frac{1}{\theta_j}\right)\phi_j \leq \frac{1-c}{c} \tag{26}$$

$$0 \leq (D_0 + D_1\theta_{j-1})\phi_{j-1} \leq \frac{1-c}{c} \tag{27}$$

$$0 \leq \left(D_1 + D_0\frac{1}{\theta_j}\right)\phi_j \leq 1 \tag{28}$$

$$0 \leq (D_0 + D_1\theta_{j-1})\phi_{j-1} \leq 1 \tag{29}$$

This leads to the following conditions on the flux limiter

$$\phi_j \leq \frac{(1-c)\theta_j}{c(D_1\theta_j + D_0)} \tag{30}$$

$$\phi_j \leq \frac{\theta_j}{\theta_j D_1 + D_0} \tag{31}$$

$$\phi_j \leq \frac{1-c}{c(D_0 + D_1\theta_j)} \tag{32}$$

$$\phi_j \leq \frac{1}{D_0 + D_1\theta_j} \tag{33}$$

When $\theta_j \leq 0$, The scheme reduces locally to first order by assuming

$$\phi_j(\theta_j) = 0 \quad for \quad \theta_j \leq 0 \tag{34}$$

The analysis for $-1 \leq c \leq 0$ goes through in exactly the same way but c is replaced by $|c|$. This establishes the theorem.

For nonlinear scalar problems the wave speed, $f'(u) = a(u)$ depends on the conservative variable. In this case we extend the previous theoretical analysis in an empirical way. The wave speed could be determined by Rankine-Hugoniot jump condition

$$a_{j+\frac{1}{2}} = \frac{f'(U_{j+1}) - f'(U_j)}{U_{j+1} - U_j} \tag{35}$$

and

$$c_{j+\frac{1}{2}} = \frac{a_{j+\frac{1}{2}}k}{h} \tag{36}$$

In the following sections we will use the method to construct second-order, third-order and fourth-order TVD schemes.

3 Second-order TVD Scheme

The fully discrete, second-order centered flux limiter scheme (Lax-Wendroff scheme) can be written as

$$U_j^{n+1} = U_j^n - \frac{k}{h}[F(U^n; j) - F(U^n; j-1)] \tag{37}$$

$$F(U^n;j) = \frac{1}{2}(F_j^n + F_{j+1}^n) - \frac{|a|}{2}\Delta U_{j+\frac{1}{2}} + \frac{|a|}{2}(1-|c|)\Delta U_{j+\frac{1}{2}}\ \phi_j \tag{38}$$

where $|c| \leq 1$ and according to equation (6), $D_0 = \frac{1}{2}(1-|c|)$ and $D_1 = 0$.

From equation (7) to (10) the flux limiter ϕ_j has to satisfy the constraints

$$\phi_j \leq \frac{2\theta_j}{|c|} \tag{39}$$

$$\phi_j \leq \frac{2\theta_j}{1-|c|} \tag{40}$$

$$\phi_j \leq \frac{2}{|c|} \tag{41}$$

$$\phi_j \leq \frac{2}{1-|c|} \tag{42}$$

which reduce to

$$\phi_j \leq \frac{2\theta_j}{\eta} \tag{43}$$

$$\phi_j \leq \frac{2}{\eta} \tag{44}$$

with

$$\begin{cases} \eta = 1-|c| & for \quad 0 \leq |c| < \frac{1}{2} \\ \eta = |c| & for \quad \frac{1}{2} \leq |c| \leq 1 \end{cases} \tag{45}$$

Equation (43) and (44) indicate that the second-order TVD region is a function of Courant number $|c|$. This conclusion is consistent with that of other researchers such as [11] and [12]. The Courant number dependent TVD regions of (43) and (44) are shown in Figure 1. The upper bound of the TVD region is the maximum for the choice of $|c| = \frac{1}{2}$. Sweby's TVD region [9] is the special case $|c| = 1$ in the Courant number dependent TVD region of Figure 1.

Using the Courant number dependent TVD region we can develop second-order Courant number dependent flux limiters. From our analysis an extension of Roe's Superbee limiter [9] is

$$\phi_j(\theta_j) = max\left[0, min\left(1, \frac{2\theta_j}{\eta}\right), min\left(\theta_j, \frac{2}{\eta}\right)\right] \tag{46}$$

which we called FD2 (Fully Discrete Second-order) limiter.

Figure 2 shows a comparison of the numerical results using Superbee (crosses), FD2 (boxes) and the exact solution (line). The initial codition consists of half a *sine* wave and a squared wave. A mesh width $\Delta x = 0.1$ is fixed. The Courant numbers used are 0.1, 0.3 and 0.5 which actualy cover the Courant number range from 0.1 to 0.9 since the TVD region is symmetric about $|c| = \frac{1}{2}$. The results are shown after 1000 time steps. As shown in the figure the performance of FD2 for the discontinuous part of the solution is superior to that of Superbee; for the smooth part of the solution they both tend to square the profile but FD2 shows less 'clipping' of the extrema. Both Superbee and FD2 are affected by the dispersive term in the truncation error which is large for small Courant numbers. The difference between Superbee and FD2 is more noticeable as the Courant number tends to $\frac{1}{2}$.

4 Third-order TVD Scheme

The 5-point third-order (both in time and space) flux limiter scheme has the following form (see [6])

$$U_j^{n+1} = U_j^n - \frac{k}{h}[F(U^n; j) - F(U^n; j-1)] \tag{47}$$

$$\begin{aligned} F(U^n; j) &= \frac{1}{2}(F_j^n + F_{j+1}^n) - \frac{|a|}{2}\Delta U_{j+\frac{1}{2}} + \left[|a|\left(\frac{1}{3} - \frac{|c|}{2} + \frac{c^2}{6}\right)\Delta U_{j+\frac{1}{2}}\right. \\ &\left. + \frac{|a|}{6}(1-c^2)\Delta U_{j+L+\frac{1}{2}}\right]\phi_j \end{aligned} \tag{48}$$

where

$$|c| \leq 1 \tag{49}$$

$$\begin{cases} L = -1 & if \quad c > 0 \\ L = 1 & if \quad c < 0 \end{cases} \tag{50}$$

and according to equation (6)

$$\begin{cases} D_0 = \frac{1}{3} - \frac{1}{2}|c| + \frac{1}{6}c^2 \\ D_1 = \frac{1}{6}(1-c^2) \end{cases} \tag{51}$$

From equations (7) to (10) the limiters are determined by

$$\phi_j \leq \frac{6\theta_j}{|c|[\theta_j(1+|c|)+2-|c|]} \tag{52}$$

$$\phi_j \leq \frac{6\theta_j}{(1-|c|)[(1+|c|)\theta_j+2-|c|]} \tag{53}$$

$$\phi_j \leq \frac{6}{|c|[\theta_j(1+|c|)+2-|c|]} \tag{54}$$

$$\phi_j \leq \frac{6}{(1-|c|)[(1+|c|)\theta_j+2-|c|]} \tag{55}$$

i.e.

$$\phi_j \leq \frac{6\theta_j}{\eta[\theta_j(1+|c|)+2-|c|]} \tag{56}$$

$$\phi_j \leq \frac{6}{\eta[\theta_j(1+|c|)+2-|c|]} \tag{57}$$

where

$$\begin{cases} \eta = 1-|c| & if \quad 0 \leq |c| < \frac{1}{2} \\ \eta = |c| & if \quad \frac{1}{2} \leq |c| \leq 1 \end{cases} \tag{58}$$

Figure 3 shows the Courant number dependent TVD regions of this scheme which has similar features to those of the second-order scheme. The upper bound of the TVD region is maximum when $|c| = \frac{1}{2}$ and minimum when $|c| = 1$. The lower bound is always $\phi = 0$.

We can define differente third-order flux limiters using the Courant number dependent TVD regions. One limiter called FD3A (Fully Discrete Third-order A) has the following form

$$\phi_j = \frac{6\theta_j}{\eta[\theta_j(1+|c|)+2-|c|]} \qquad if \quad 0 \leq \theta_j < \theta^L \tag{59}$$

$$\phi_j = 1 \qquad if \quad \theta^L \leq \theta_j \leq \theta^R \tag{60}$$

$$\phi_j = \frac{6}{\eta[\theta_j(1+|c|)+2-|c|]} \qquad if \quad \theta_j > \theta^R \tag{61}$$

$$\phi_j = 0 \qquad if \quad \theta_j < 0 \tag{62}$$

where

$$\theta^L = \frac{\eta(2-|c|)}{6-\eta(1+|c|)} \tag{63}$$

$$\theta^R = \frac{6-\eta(2-|c|)}{\eta(1+|c|)} \tag{64}$$

Figure 4 shows the FD3A limiter for three values of Courant number. They are given by the full lines.

Figure 5 shows the performance of the limiter after 50 time steps with Courant numbers 0.1, 0.3 and 0.5. The solid line is the exact solution. As shown in the figure the numerical results (boxes) look very good in the smooth part but discontinuities are smeared with 4-5 interior points. We are interested in the behaviour for long time evolution. Figure 6 shows the results after 1000 time steps which shows that this limiter is not very satisfactory for long times. It introduces too much numerical diffusion due to the imposion of the TVD property, whereby the scheme reduces locally to first order.

The authors would suggest the following empirical limiter, called FD3B (Fully Discrete Third-order B)

$$\phi_j = \frac{6\theta_j}{\eta[\theta_j(1+|c|)+2-|c|]} \quad if \;\; 0 \le \theta_j < (1.1\eta - 0.17) \tag{65}$$

$$\phi_j = 1 \quad if \;\; (1.1\eta - 0.17) \le \theta_j \le (2.78 - 1.4\eta) \tag{66}$$

$$\phi_j = \frac{6}{\eta[\theta_j(1+|c|)+2-|c|]} \quad if \;\; \theta_j > (2.78 - 1.4\eta) \tag{67}$$

$$\phi_j = 0 \quad if \;\; \theta_j < 0 \tag{68}$$

Figure 7 shows the FD3B limiter for Courant number 0.5.

Figures 8 and 9 show the comparison of the numerical results of the limiter (boxes) and the exact solution (line) after 50 and 1000 time steps respectively with Courant numbers 0.1, 0.3 and 0.5. These figures show that the numerical results of FD3B are far superior to those obtaind with FD3A. There is virtually no numerical diffusion but some tendency to 'square' the smooth parts is observed. For $|c|$ close to $\frac{1}{2}$ the results are very good for both the smooth and discontinuous parts of the solution. We can expect that the fully discrete (both in space and time) third-order flux limiter scheme (FD3B) will give good performance for most practical flows.

5 Fourth-order TVD Scheme

The five-point, fourth-order (both in time and space) centered flux limiter scheme can be written as (refer to [6])

$$U_j^{n+1} = U_j^n - \frac{k}{h}[F(U^n; j) - F(U^n; j-1)] \tag{69}$$

$$\begin{aligned} F(U^n; j) &= \frac{1}{2}(F_j^n + F_{j+1}^n) - \frac{|a|}{2}\Delta U_{j+\frac{1}{2}} + \left[a\ D_{j+\frac{1}{2}}\Delta U_{j+\frac{1}{2}} + a\ D_{j+L+\frac{1}{2}}\Delta U_{j+L+\frac{1}{2}}\right]\ \phi_j \\ &\quad + a\ D_{j+M+\frac{1}{2}}\Delta U_{j+M+\frac{1}{2}}\ \phi_{j+M} \end{aligned} \tag{70}$$

where

$$\begin{cases} D_{j-\frac{1}{2}} = \frac{1}{12} + \frac{1}{24}c - \frac{1}{12}c^2 - \frac{1}{24}c^3 \\ D_{j+\frac{1}{2}} = \frac{1}{2}\ sgn(a) - \frac{7}{12}c + \frac{1}{12}c^3 \\ D_{j+\frac{3}{2}} = \frac{1}{12}c^2 + \frac{1}{24}c - \frac{1}{12} - \frac{1}{24}c^3 \end{cases} \tag{71}$$

$$\begin{cases} L = -1, \quad M = 1 \quad if \quad c > 0 \\ L = 1, \quad M = -1 \quad if \quad c < 0 \end{cases} \tag{72}$$

$$|c| \leq 1 \tag{73}$$

This is a two limiter scheme. Since it is difficult to obtain an analytical expression for the limiters we determine the limiters by a semi-empirical method, namely, the first limiter ϕ_j is obtained by equations (7) to (10) and the second one ϕ_{j+M} is defined by experimentation. Therefore ϕ_j has to satisfy the following condition

$$\phi_j \leq \frac{24\theta_j}{\eta[(2+|c|)(1+|c|)\theta_j + 2(6-|c|) - 2c^2]} \tag{74}$$

$$\phi_j \leq \frac{24}{\eta[(2+|c|)(1+|c|)\theta_j + 2(6-|c|) - 2c^2]} \tag{75}$$

where

$$\begin{cases} \eta = 1 - |c| \quad for \quad 0 \leq |c| < \frac{1}{2} \\ \eta = |c| \qquad for \quad \frac{1}{2} \leq |c| \leq 1 \end{cases} \tag{76}$$

The second empirical limiter satisfies the following constraint

$$\phi_{j+M} \leq A(c)\ \theta_{j+M} \tag{77}$$

Here the coefficient $A(c)$ is determined by experiment.

The following limiters called FD4 have been tried by the authors

$$\phi_j = \frac{24\theta_j}{\eta[(2+|c|)(1+|c|)\theta_j + 2(6-|c|) - 2c^2]} \quad for \;\; 0 \le \theta_j < \theta^L \tag{78}$$

$$\phi_j = 1 \quad for \;\; \theta^L \le \theta_j \le \theta^R \tag{79}$$

$$\phi_j = \frac{24}{\eta[(2+|c|)(1+|c|)\theta_j + 2(6-|c|) - 2c^2]} \quad for \;\; \theta_j > \theta^R \tag{80}$$

$$\phi_j = 0 \quad for \;\; \theta_j < 0 \tag{81}$$

where

$$\theta^L = \eta \tag{82}$$

$$\theta^R = 3.55 - 1.5\eta \tag{83}$$

and

$$\phi_{j+M} = \eta\,\theta_{j+M} \quad for \;\; 0 \le \theta_{j+M} < \frac{1}{2} \tag{84}$$

$$\phi_{j+M} = 1 \quad for \;\; \phi_{j+M} > \frac{1}{2} \tag{85}$$

$$\phi_{j+M} = 0 \quad for \;\; \phi_{j+M} < 0 \tag{86}$$

Figures 10 and 11 show comparisons of the numerical results (boxes) and the exact solution (line) after 50 and 1000 time steps respectively, with Courant number 0.1, 0.3 and 0.5 . The results indicate that the FD4 limiter is good for short time evolution. For long time evolution it is good for discontinuities, but is not satisfactory for the smooth parts.

Another approach is to use a hybrid flux limiter method following the flux corrected transport approach whereby the fourth-order flux $F^{(4)}(U;j)$ (equation (70) without limiters) can be written as

$$F(U;j) = F^{(3)}(U;j) + [F^{(4)}(U;j) - F^{(3)}(U;j)]\;\phi_j^* \tag{87}$$

where $F^{(3)}$ is the third-order flux which includes a limiter ϕ_j and ϕ_j^* is an empirical flux limiter. The limiter ϕ_j^* is unity in smooth regions, which makes the flux (87)

fourth-order accurate. In regions of high gradients ϕ_j^* is zero, which means that the flux (87) reduces to third-order accuracy.

In order to determine ϕ_j^* we need first to define the locally smooth regions for flux (87). If we utilize the information provided by the third-order TVD method with FD3A limiter (Fig. 4), the 'smooth' region might be given by equation (60), that is

$$\frac{\eta(2-|c|)}{6-\eta(1+|c|)} \leq \theta_j \leq \frac{6-\eta(2-|c|)}{\eta(1+|c|)}$$

gives oscillation free solutions.

Since the flux (87) involves three intercell boundaries ($j-\frac{1}{2}$, $j+\frac{1}{2}$, $j+\frac{3}{2}$), locally smooth regions for the flux (87) means that in all of these cells the function must be smooth. Therefore the empirical flux limiter ϕ_j^* is determined by

$$\phi_j^* = 1 \quad if \quad \begin{cases} \frac{\eta(2-|c|)}{6-\eta(1+|c|)} \leq \theta_j^L \leq \frac{6-\eta(2-|c|)}{\eta(1+|c|)} \\ \frac{\eta(2-|c|)}{6-\eta(1+|c|)} \leq \theta_j^R \leq \frac{6-\eta(2-|c|)}{\eta(1+|c|)} \end{cases} \tag{88}$$

$$\phi_j^* = 0 \quad otherwise \tag{89}$$

where

$$\left.\begin{cases} \theta_j^L = \frac{\Delta U_{j-\frac{1}{2}}}{\Delta U_{j+\frac{1}{2}}} \\ \theta_j^R = \frac{\Delta U_{j+\frac{1}{2}}}{\Delta U_{j+\frac{3}{2}}} \end{cases} \quad for \quad c>0 \right\}$$

$$\left.\begin{cases} \theta_j^L = \frac{\Delta U_{j+\frac{3}{2}}}{\Delta U_{j+\frac{1}{2}}} \\ \theta_j^R = \frac{\Delta U_{j+\frac{1}{2}}}{\Delta U_{j-\frac{1}{2}}} \end{cases} \quad for \quad c<0 \right\} \tag{90}$$

Figures 12 and 13 show comparisons of the exact solution (line) and the numerical results (symbol) obtained by the fourth-order scheme with flux (87) after 50 and 1000 time steps respectively. The third-order flux $F^{(3)}$ uses FD3A limiter (equation (59)-(64)). By comparing the fourth-order results to the corresponding third-order results of Figures 5 and 6 one can see a remarkable improvement in accuracy partially for $|c|$ close to $\frac{1}{2}$. The improvement is observed for both smooth parts of the solution and near discontinuities. Also, the improvement holds for long time evolution.

The hybrid-limiting approach of equation (87) appears to provide a satisfactory way

of dealing with high-order schemes. In general, for an m-th order scheme we write

$$F(U;j) = F^{(3)}(U;j) + [F^{(m)}(U;j) - F^{(3)}(U;j)]\ \phi_j^* \tag{91}$$

where the basic scheme $F^{(3)}$ is third-order accuracy in smooth parts and has a limiter which is theoretically sound. The only empirical aspect comes in the choice of ϕ_j^*, but the approach suggested utilises the theory for the third-order scheme to detect smooth regions, in which ϕ_j^* is set to unity, giving in this way the m-th order scheme.

6 Conclusions

Courant-number dependent TVD regions for second and third-order schemes have been theoretically established. Flux limiters have been proposed and tested via numerical experiments. For methods of m-th order accuracy (m $\geq$ 4) we proposed a semi-empirical limiting procedure that appears to work well. Tests on the case of m=4 give very satisfactory results.

References

[1] **LEVEQUE, R.J.,** 1990, Numerical Methods for Conservation Laws. Birkhauser.

[2] **VAN LEER, B.,** 1974-1979, Towards the Ultimate Conservative Difference Scheme. 2(1974), 3(1977), 4(1977), 5(1979), J. Comput. Phys.

[3] **HARTEN, A. and OSHER, S.,** 1987, Uniformly High-order Accurate Non-oscillatory Schemes 1. SIAM J. Num. Anal., 24, pp. 279-309.

[4] **SHU, S. and OSHER, S.,** 1988, Efficient Implementation of Essentially Non-oscillatory Shock Capturing Schemes. J. Comput. Phys., 77, pp. 439-471.

[5] **HARTEN, A.,** 1989, ENO Schemes with Subcell Resolution. J. Comput. Phys., 83, pp. 148-184.

[6] **SHI, J. and TORO, E.F.**, 1993, Fully Discrete High-order Schemes for a Scalar Hyperbolic Conservation Law. COA Report No. 9307, Cranfield Institute of Technology, Cranfield, U.K..

[7] **SHI, J.**, 1993, A Simplified Von Neumann Method for Linear Stability Analysis. COA Report No. 9310, Cranfield Institute of Technology, Cranfield, U.K..

[8] **HARTEN, A.**, 1983, High Resolution Schemes for Hyperbolic Conservation Laws. J. Comput. Phys., 49, pp. 357-393.

[9] **SWEBY, P.K.**, 1984, High Resolution Schemes Using Flux Limiters for Hyperbolic Conservation Laws. SIAM J. Num. Anal., 21, pp 995-1011.

[10] **ROE, P.L.**, 1987, Numerical Algorithms for the Linear Wave Equation. Royal Aircraft Establishment Technical Report 81047.

[11] **LEONARD, B.P.**, 1988, Universal Limiter for Transient Interpolation Modeling of the Advective Transport Equations: The ULTIMATE Conservative Difference Scheme. NASA Technical Memorandum 100916.

[12] **ROE, P.L.**, 1984, Generalized Formulation of TVD Lax-Wendroff Schemes. NASA Contractor Report No. 84-53.

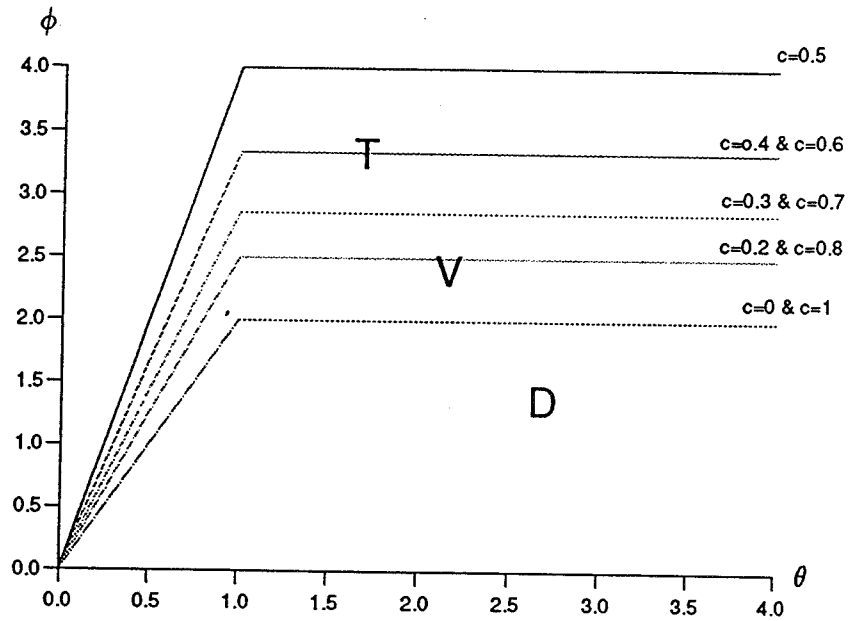

Figure 1: Courant Number Dependent Second-order TVD Region

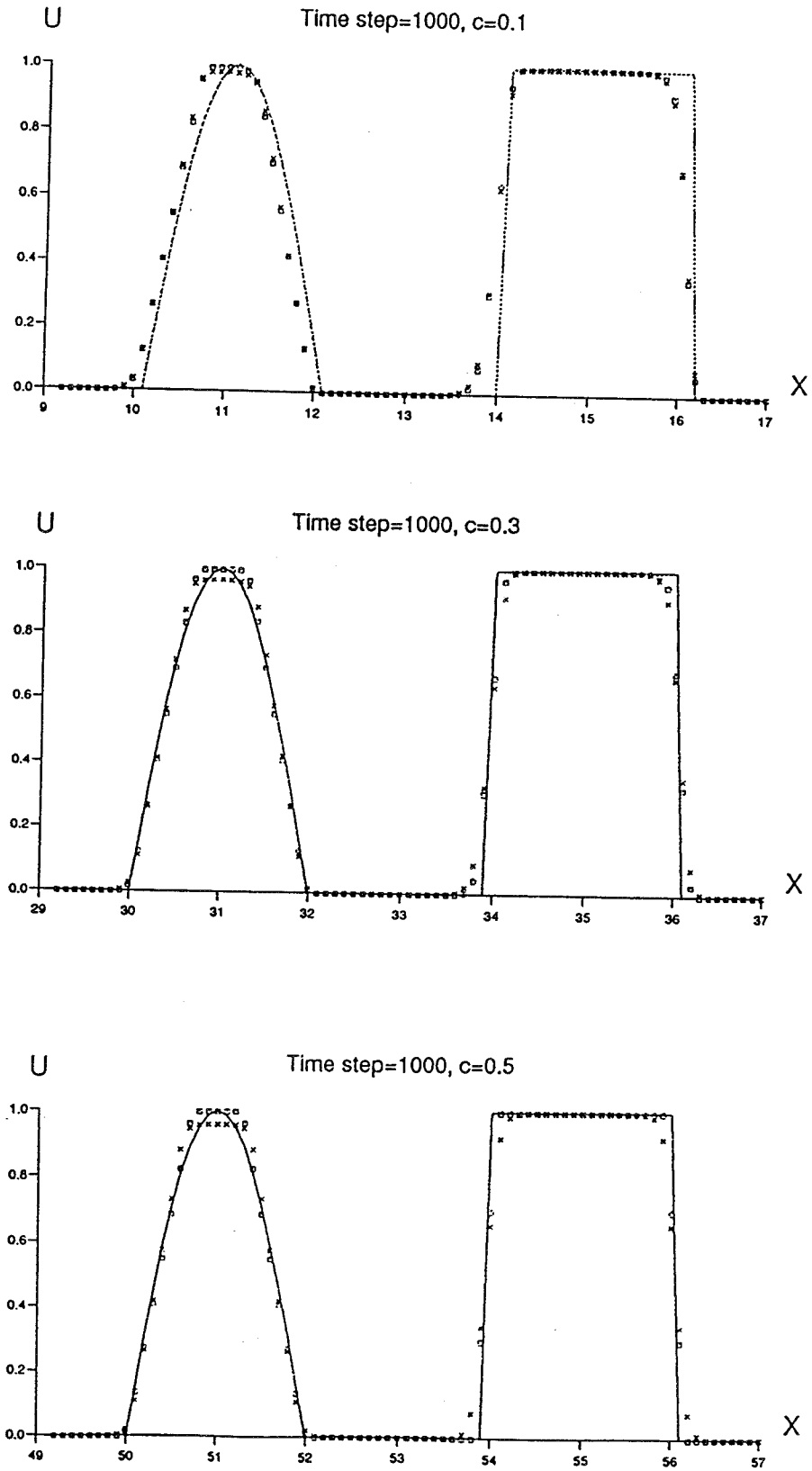

Figure 2: Comparison between the Exact Solution (line) and the Numerical Results Using Superbee (crosses) and FD2 (boxes) after 1000 Time Steps

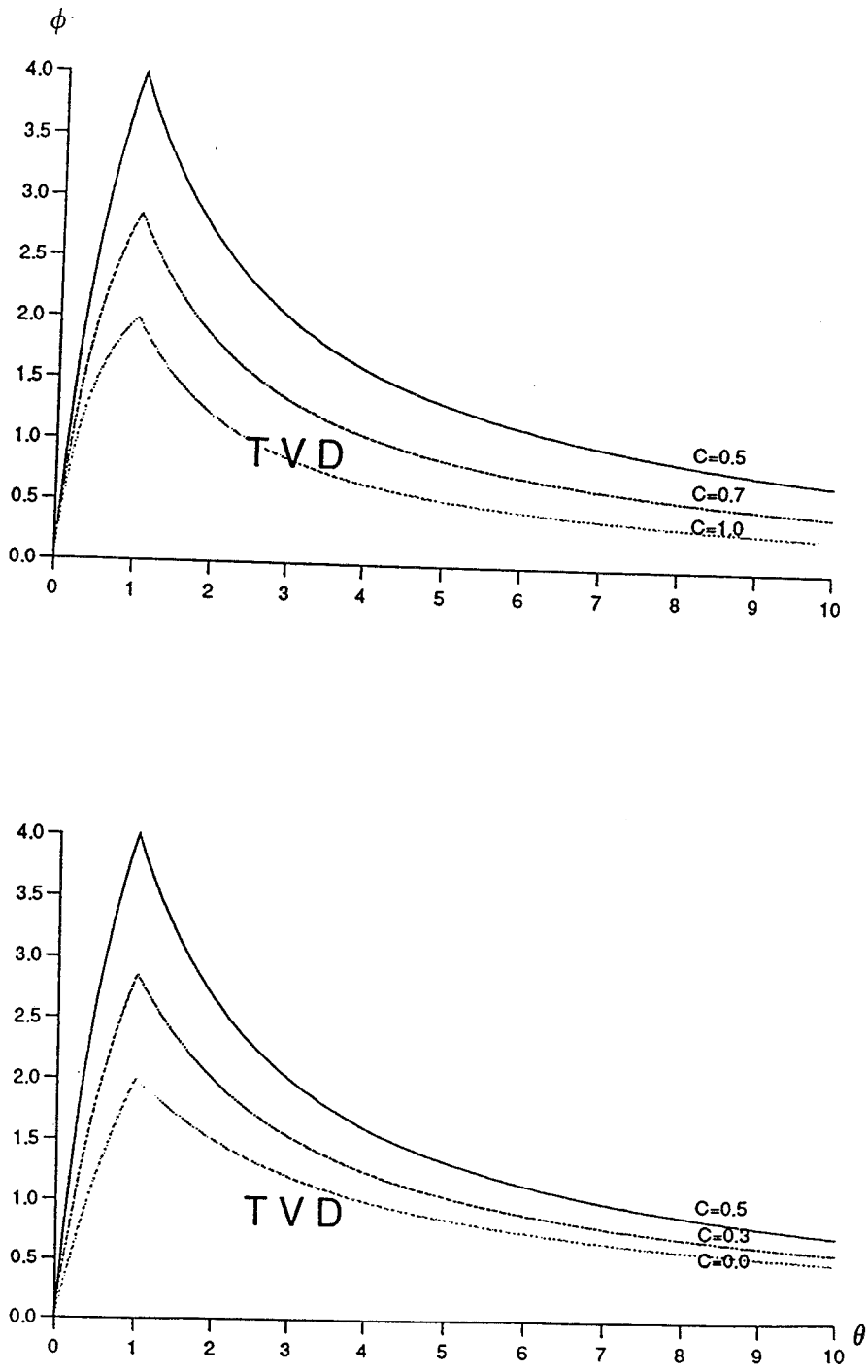

Figure 3: Courant Number Dependent Third-order TVD Region

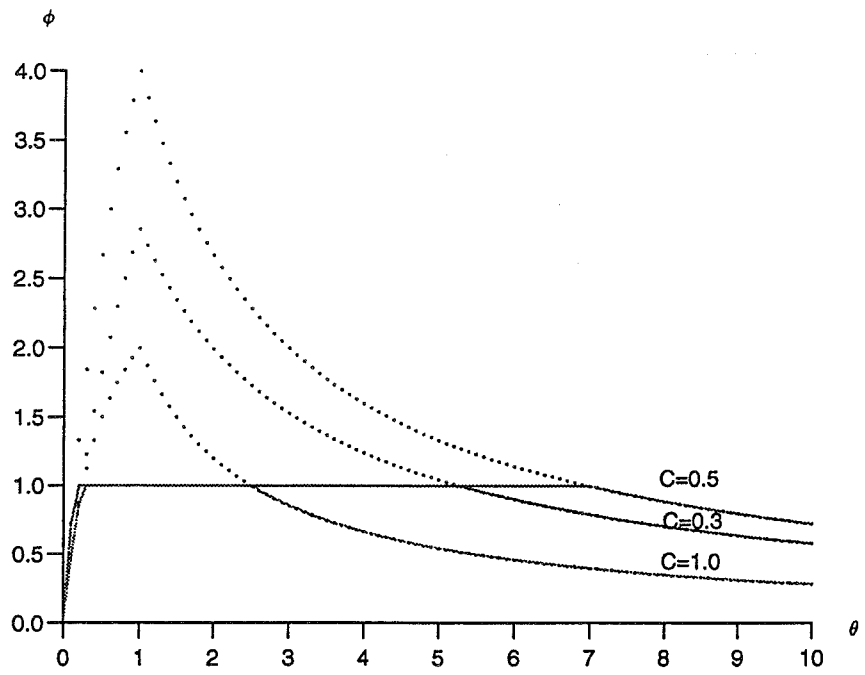

Figure 4: FD3A Limiter with Courant Number 0.1, 0.3 and 0.5 (lines)

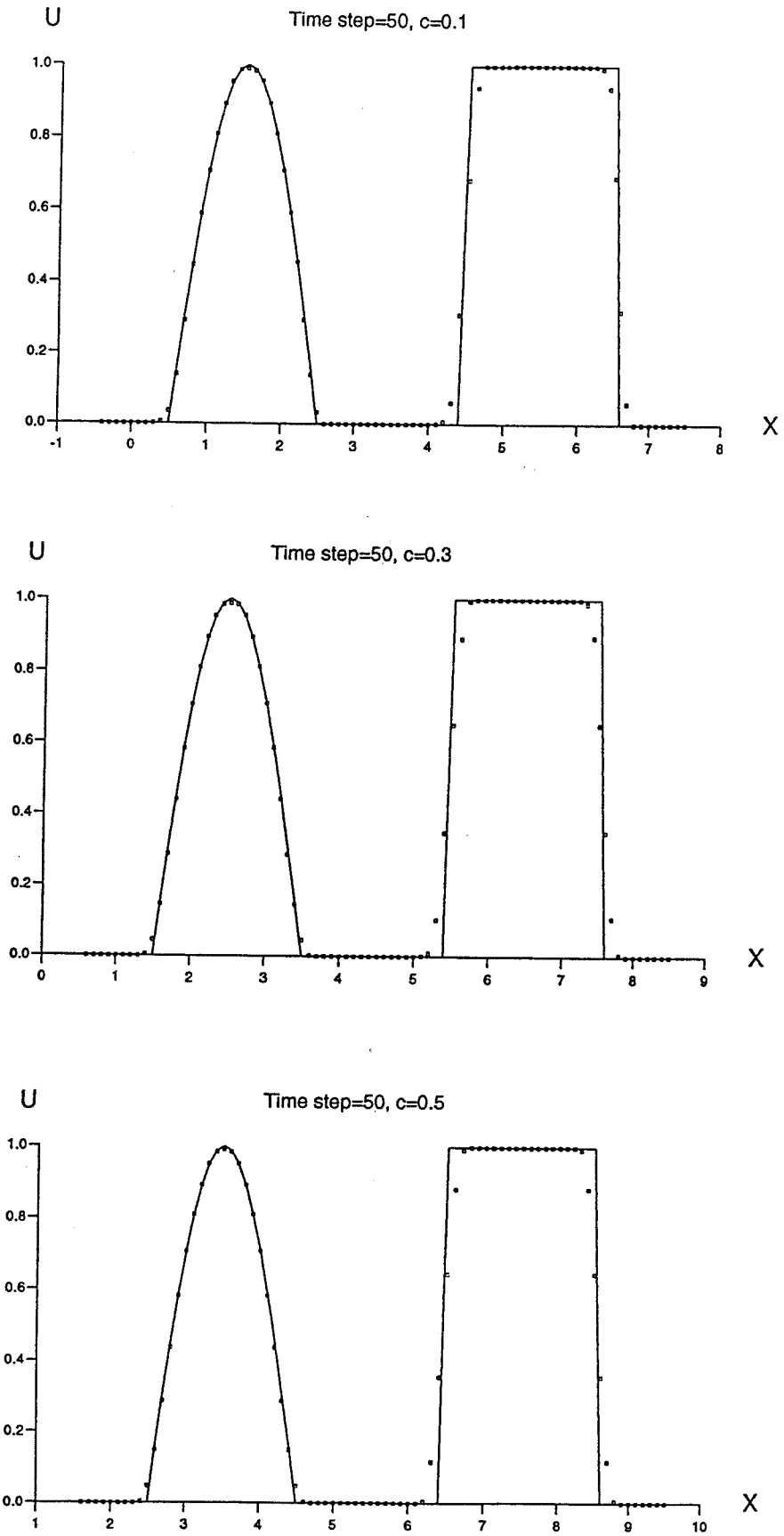

Figure 5: Comparision between the Exact Solution (line) and the Numerical Results of FD3A (crosses) after 50 Time Steps

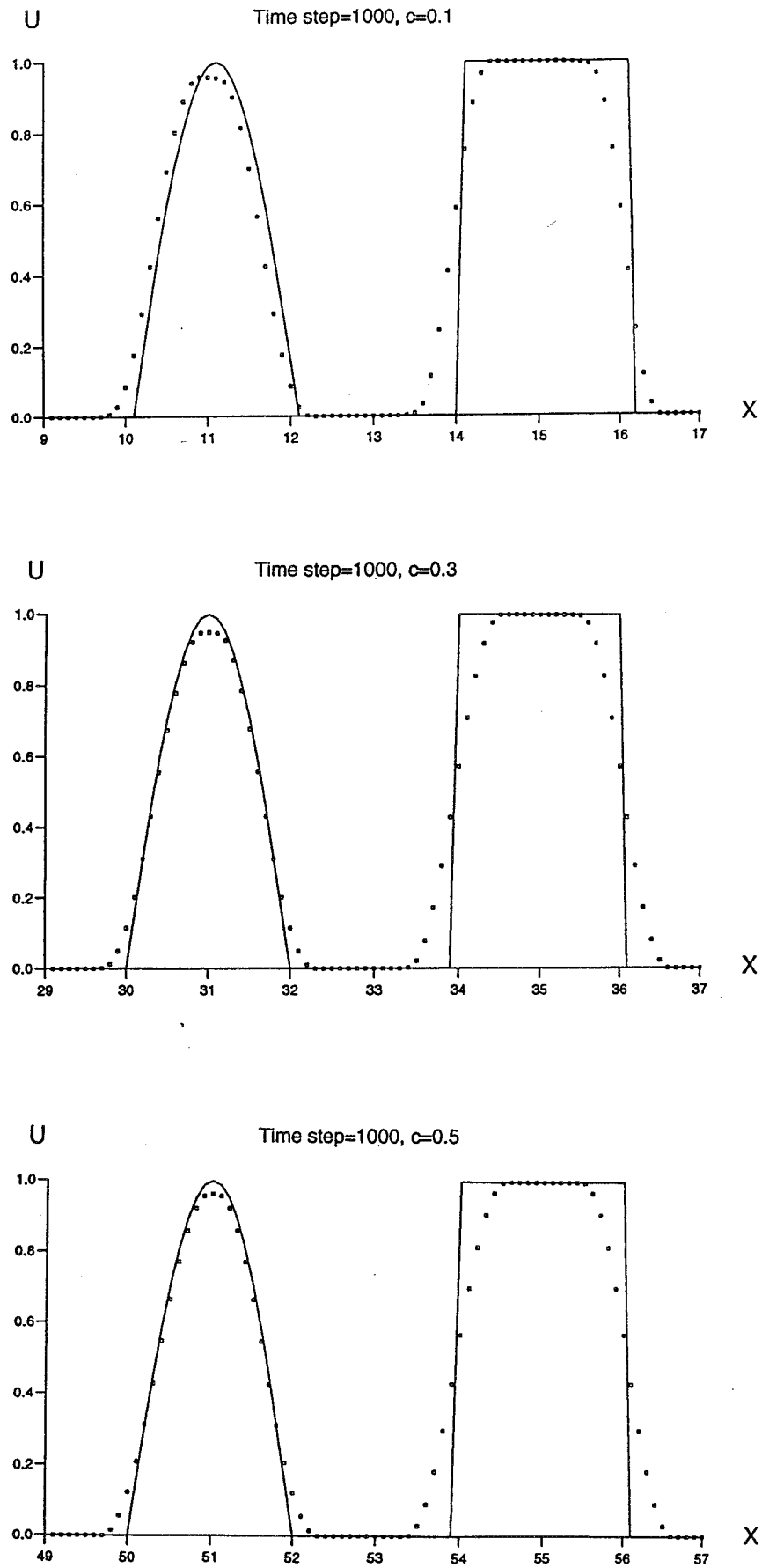

Figure 6: Comparison between the Exact Solution (line) and the Numerical Results of FD3A (crosses) after 1000 Time Steps

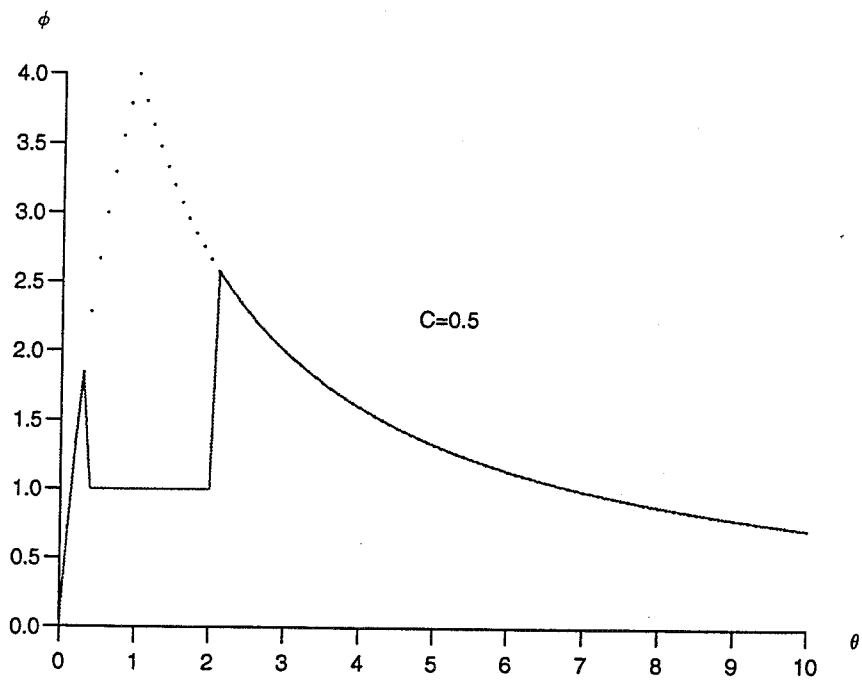

Figure 7: FD3B Limiter with Courant Number 0.5 (lines)

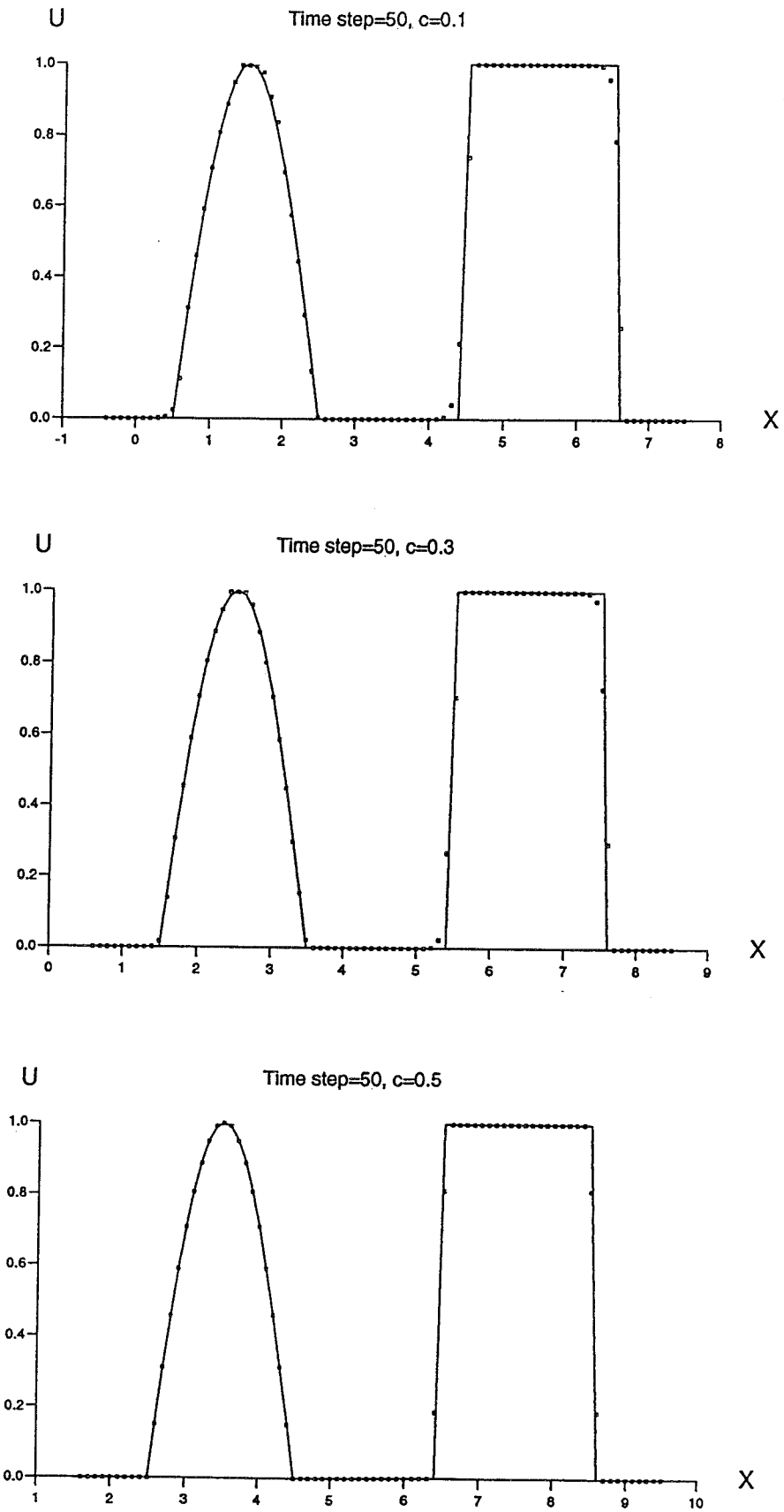

Figure 8: Comparison between the Exact Solution (line) and the Numerical Results of FD3B (crosses) after 50 Time Steps

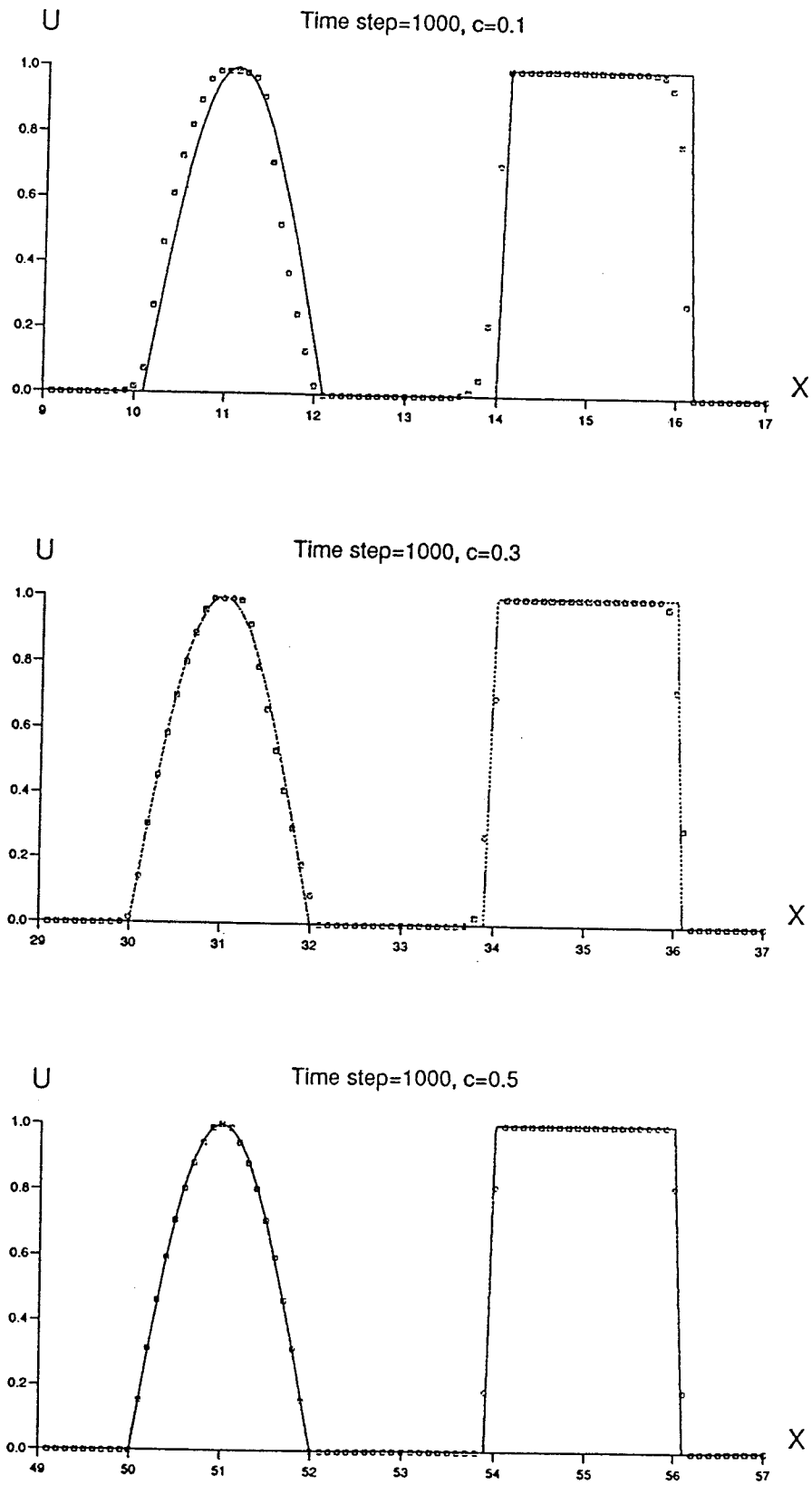

Figure 9: Comparison between the Exact Solution (line) and the Numerical Results of FD3B (crosses) after 1000 Time Steps

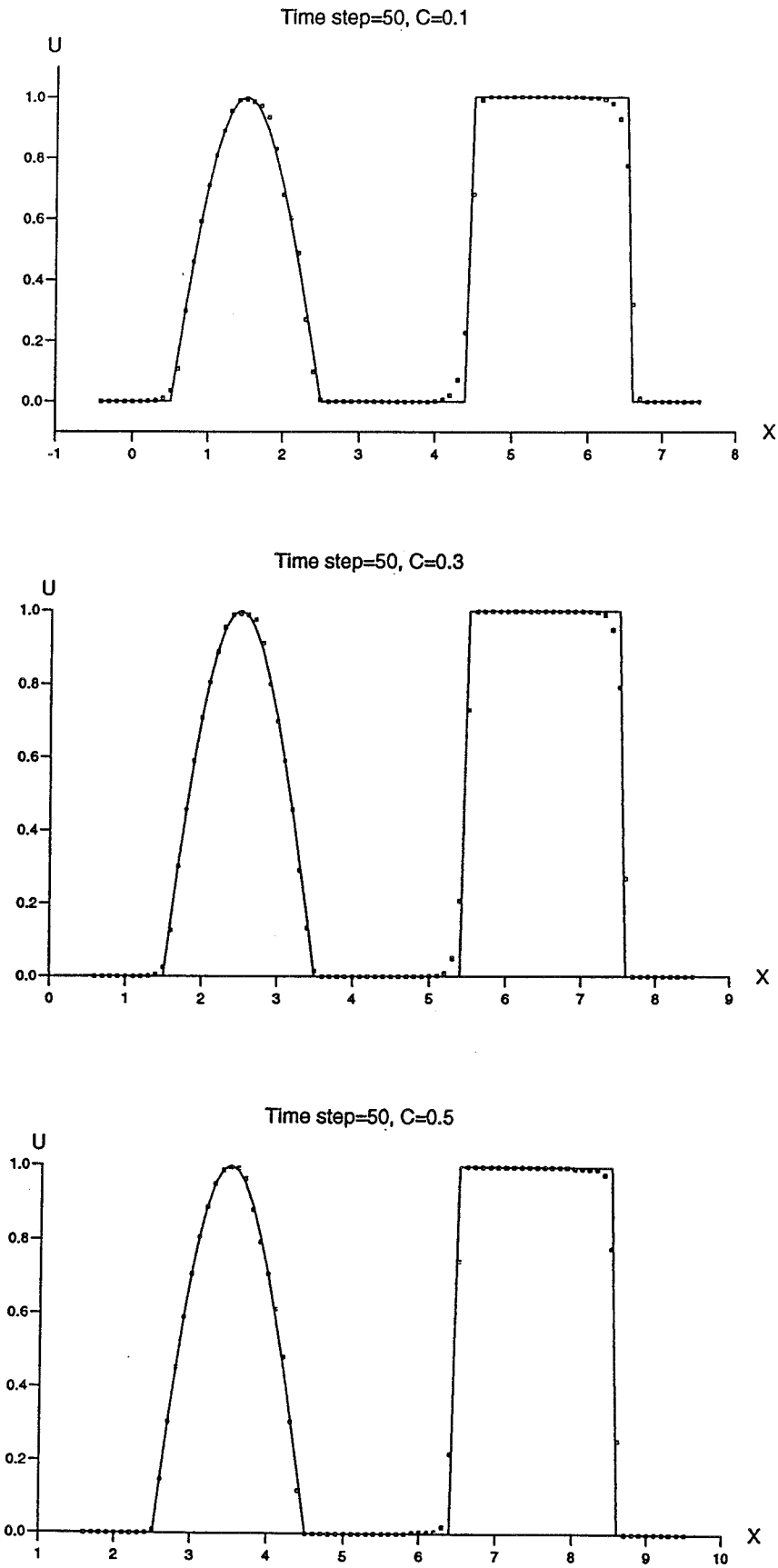

Figure 10: Comparison between the Exact Solution (line) and the Numerical Results of FD4 (crosses) after 50 Time Steps

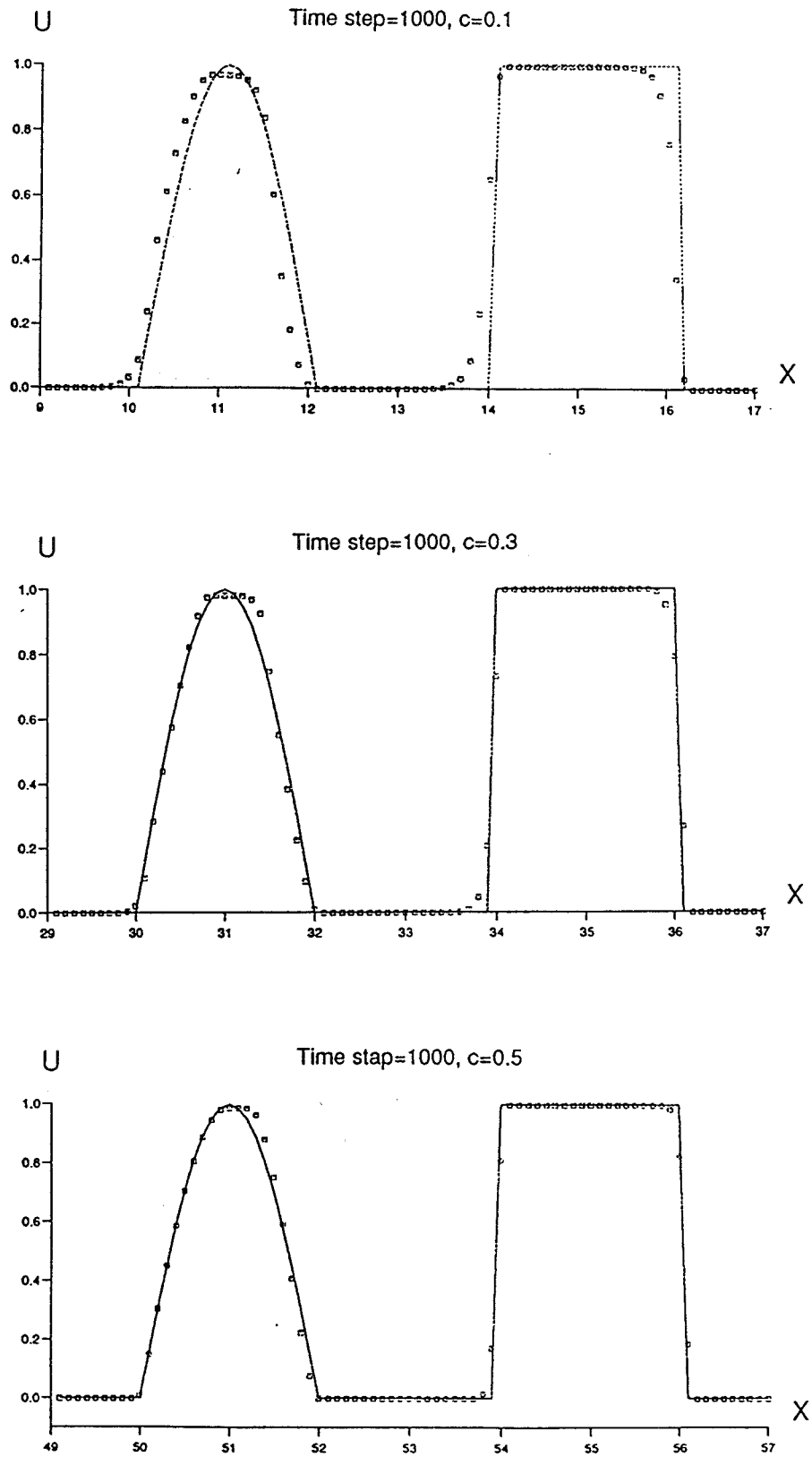

Figure 11: Comparison between the Exact Solution (line) and the Numerical Results of FD4 (crosses) after 1000 Time Steps

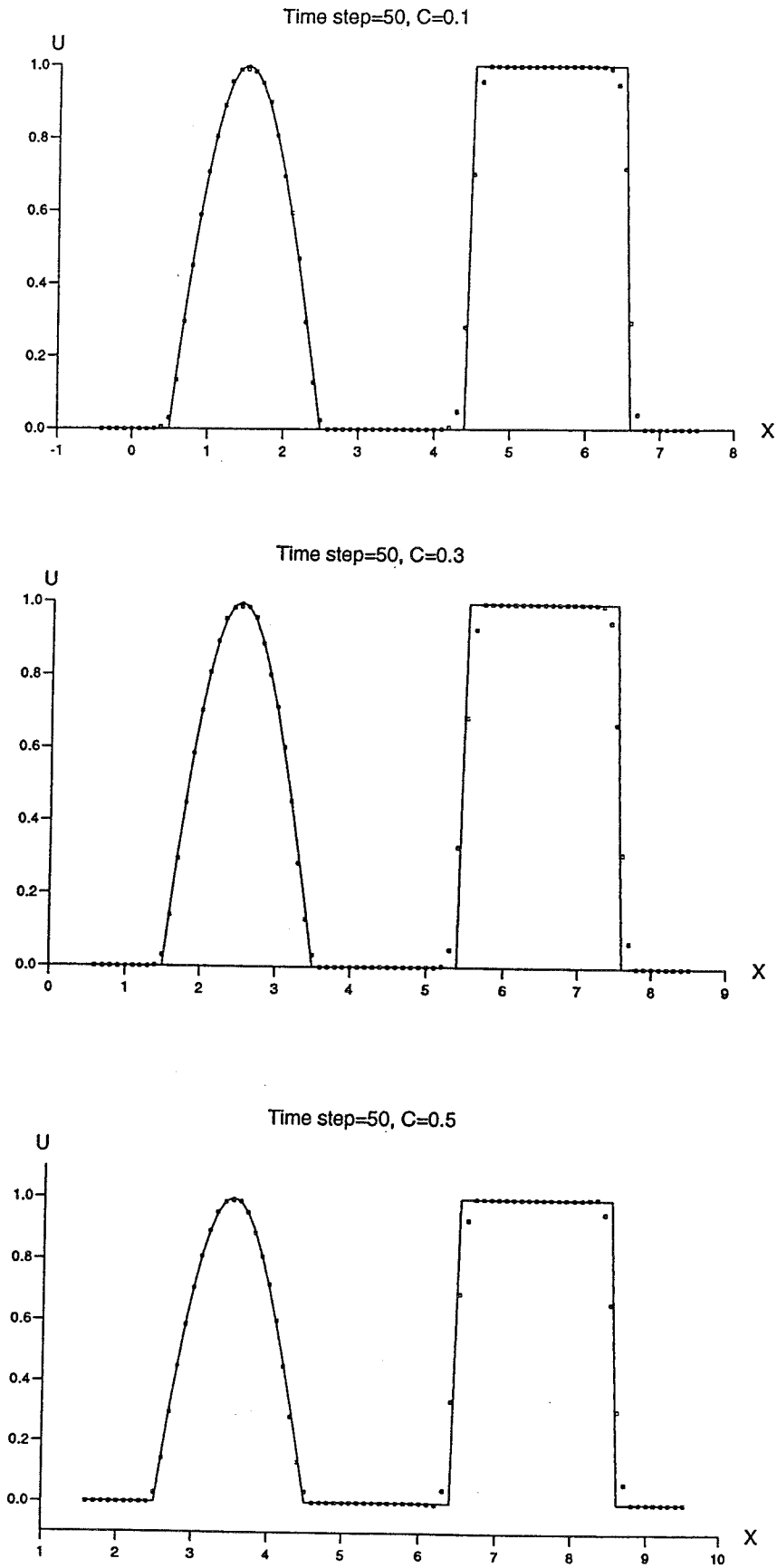

Figure 12: Comparison between the Exact Solution (line) and the Numerical Results of the Hybrid Method (crosses) after 50 Time Steps

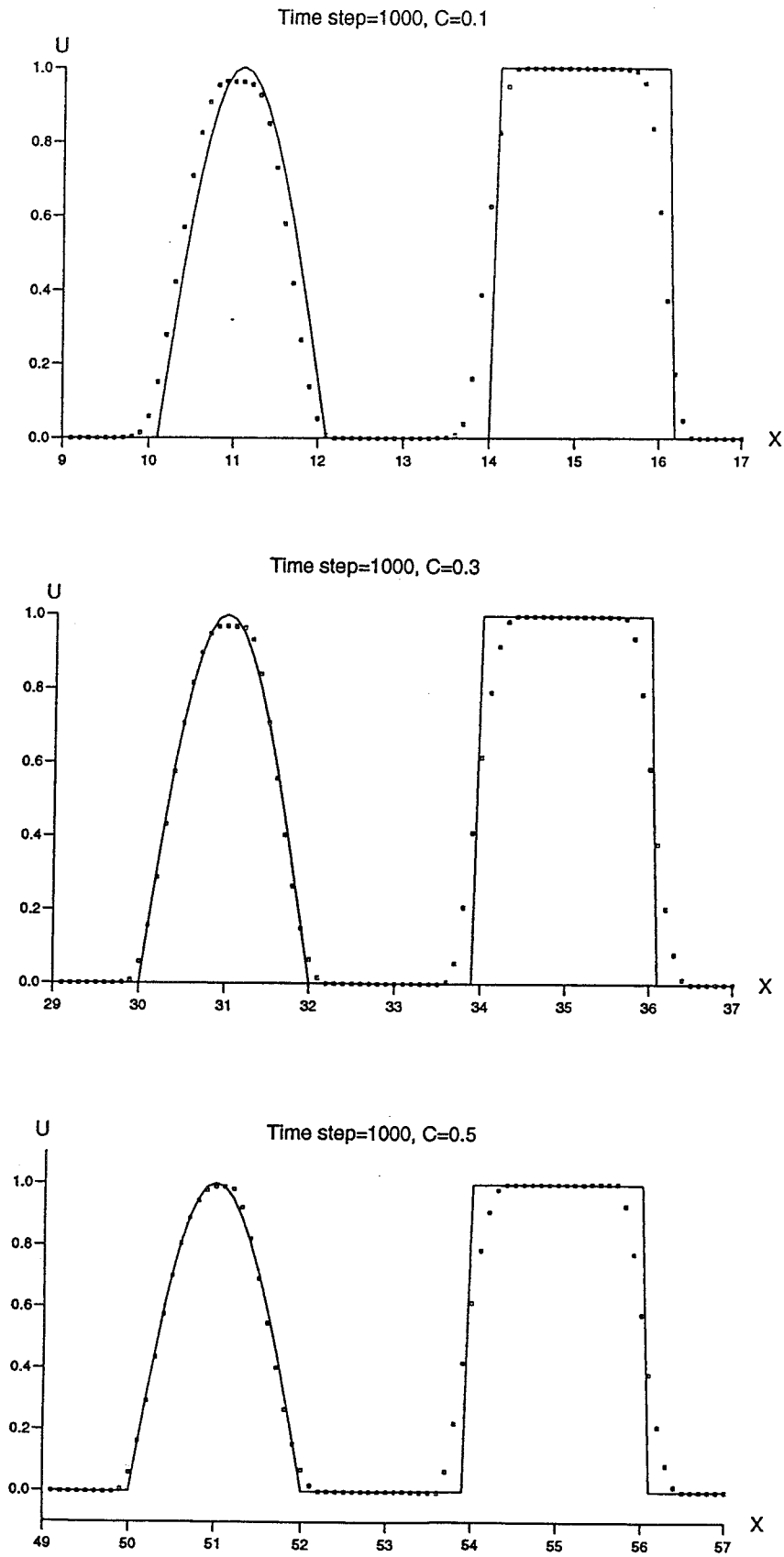

Figure 13: Comparison between the Exact Solution (line) and the Numerical Results of the Hybrid Method (crosses) after 1000 Time Steps